

# Graphene Oxide Substrate Promotes Neurotrophic Factor Secretion and Survival of Human Schwann-Like Adipose Mesenchymal Stromal Cells

Steffan H. Llewellyn, Alessandro Faroni, Maria Iliut, Cian Bartlam, Aravind Vijayaraghavan, and Adam J. Reid\*


Mesenchymal stromal cells from adipose tissue (AD-MSCs) exhibit favorable clinical traits for autologous transplantation and can develop 'Schwann-like' phenotypes (sAD-MSCs) to improve peripheral nerve regeneration, where severe injuries yield insufficient recovery. However, sAD-MSCs regress without biochemical stimulation and detach from conduits under unfavorable transplant conditions, negating their paracrine effects. Graphene-derived materials support AD-MSC attachment, regulating cell adhesion and function through physiochemistry and topography. Graphene oxide (GO) is a suitable substrate for human sAD-MSCs incubation toward severe peripheral nerve injuries by evaluating transcriptome changes, neurotrophic factor expression over a 7-days period, and cell viability in apoptotic conditions is reported. Transcriptome changes from GO incubation across four patients are minor compared to biological variance. Nerve growth factor (NGF), brain-derived neurotrophic factor (BDNF), and glial-derived neurotrophic factor (GDNF) gene expression is unchanged from sAD-MSCs on GO substrates, but NGF and GDNF protein secretion increase at day 3 and 7. Secretome changes do not improve dorsal root ganglia neuron axon regeneration in conditioned media culture models. Fewer sAD-MSCs detach from GO substrates compared to glass following phosphate buffer saline exposure, which simulates apoptotic conditions. Overall, GO substrates are compatible with sAD-MSC primed for peripheral nerve regeneration strategies and protect the cell population in harsh environments.

## 1. Introduction

Severe peripheral nerve injury (PNI) results in lesions necessitating surgical intervention, which may require healthy nerve transplantation to bridge the gap. These procedures cause donor site morbidity and poor functional recovery, prompting need for alternative methods. Combining autologous cell therapy with functional materials to develop bioengineered conduits are feasible strategies to instigate recovery and improve patient outcome. Following injury, Schwann cells (SCs) trigger regeneration by transitioning to a repair phenotype, which increase neurotrophic factor (neurotrophin) production, secrete cytokines to recruit macrophages and develop extracellular matrix (ECM) to provide outgrowing neurites structural support.<sup>[1]</sup> Though autologous SCs are effective, functional nerves are sacrificed to provide low expansion cells, making them problematic clinical candidates.<sup>[2]</sup>

Multipotent, mesenchymal stromal cells are promising alternatives due to their regenerative paracrine action, ease of maintenance in vitro, and clinical safety.<sup>[3]</sup>

Dr. S. H. Llewellyn, Dr. A. Faroni, Dr. A. J. Reid  
Blond McIndoe Laboratories  
Division of Cell Matrix Biology and Regenerative Medicine  
School of Biological Sciences  
Faculty of Biology Medicine and Health  
University of Manchester  
Manchester Academic Health Science Centre  
Manchester M13 9PL, UK  
E-mail: Adam.Reid@manchester.ac.uk

 The ORCID identification number(s) for the author(s) of this article can be found under <https://doi.org/10.1002/adbi.202000271>.

© 2021 The Authors. Advanced Biology published by Wiley-VCH GmbH. This is an open access article under the terms of the Creative Commons Attribution License, which permits use, distribution and reproduction in any medium, provided the original work is properly cited.

Dr. S. H. Llewellyn, Dr. M. Iliut, Dr. C. Bartlam, Dr. A. Vijayaraghavan  
Department of Materials and National Graphene Institute  
The University of Manchester  
Manchester M13 9PL, UK

Dr. C. Bartlam  
Institute of Physics  
EIT 2  
Bundeswehr University Munich  
Neubiberg 85577, Germany

Dr. A. J. Reid  
Department of Plastic Surgery & Burns  
Wythenshawe Hospital  
Manchester University NHS Foundation Trust  
Manchester Academic Health Science Centre  
Manchester M23 9LT, UK

DOI: 10.1002/adbi.202000271

Mesenchymal stromal cells from adipose tissue (AD-MSCs) are harvested from an accessible, abundant source and demonstrate compatibility with common nerve conduit materials.<sup>[4]</sup> AD-MSCs constitutively secrete nerve growth factor (NGF), brain-derived neurotrophic factor (BDNF), and glial-derived neurotrophic factor (GDNF), but neurotrophin production increases when they are stimulated toward a “Schwann-like” phenotype (sAD-MSC) using biochemical stimulation.<sup>[5]</sup> Unlike the non-stimulated phenotype, sAD-MSC exhibit myelinating features *in vivo* and upregulate myelinating factors such as Krox20, which translates to improved PNI regeneration.<sup>[6,7]</sup> However, human sAD-MSCs rapidly regress to their original phenotype once stimulants are withdrawn.<sup>[8]</sup> Moreover, sAD-MSC therapeutic effects require crosstalk with damaged nerves, yet *in vivo* results indicate a substantial proportion seeded in conduits detach and migrate from the site of injury over several days due to the harsh transplant environment, thus failing to capitalize on paracrine intervention strategies.<sup>[9]</sup> Progress with human sAD-MSCs as therapeutics for severe PNI requires strategies to improve stimulation, negate phenotype regression, and address detachment.

Stem cell fate *in vitro* can be influenced by environmental cues from nanoscale properties of incubation material. Nanotopography not only impacts MSC stemness or promote differentiation, but it can do so in absence of conventional biochemical stimulus *in vitro*.<sup>[10]</sup> Moreover, material chemistry and nanoscale features are factors that influence ECM adsorption, consequently impacting MSC attachment, proliferation and downstream differentiation.<sup>[11]</sup> Graphene is a 2D material consisting of one-atom thick carbon lattice researched across numerous scientific disciplines including tissue engineering, as a result of its physicochemical properties.<sup>[12]</sup> Graphene and its derived materials, such as graphene oxide (GO), have been studied as an interface in peripheral nerve research.<sup>[13]</sup> Though lacking pristine graphene’s conductivity, GO physiochemistry is a desirable trait for incubation material, shown to impact MSC proliferation and mesodermal differentiation.<sup>[14]</sup> Additionally, graphene-derived materials influence ECM protein production, improving MSC adhesion and potentially providing greater detachment resistance.<sup>[15]</sup>

We previously reported sAD-MSC increased expression for neurotrophins and their corresponding receptors as well as cytoskeleton genes linked to glial differentiation when incubated on GO substrates *in vitro*.<sup>[16]</sup> Results were limited to 48 h, meaning sAD-MSC effects on sAD-MSC regression after longer exposure and therapeutic analysis were not made. We hypothesize GO platforms continue to stimulate sAD-MSC transition, slowing “Schwann-like” regression and improving regenerative capacity, making GO substrate desirable for severe PNI research. To test material suitability for autologous therapy, transcriptome and cell viability was measured from sAD-MSCs originating from different patient-samples. Neurotrophin gene and protein expression were measured at day 3 and day 7, following growth factor supplementation, to evaluate sAD-MSC stimulation and regression. Functional therapeutic changes were measured using an *in vitro* model of neuronal PNI recovery. Finally, to test cell-detachment effects on GO substrate sAD-MSC were placed under stress conditions *in vitro* using a harsh saline environment.

## 2. Experimental Section

All reagents were purchased from Sigma-Aldrich (Poole, UK) unless otherwise stated.

### 2.1. Graphene Oxide Characterization and Substrate Preparation

GO solution was prepared via the modified Hummers method, following the protocol outlined in Wychowanec et al.<sup>[17]</sup> The final GO material was washed via centrifugation ( $15000 \times g$ , 1 h) using sterile, cell-culture grade H<sub>2</sub>O to develop a platform suitable for culture conditions. Prior to substrate development, physical and chemical properties of GO flakes were measured. SiO<sub>2</sub> wafers (Alpha Nanotech, UK) were cleaned in acetone under sonication (20 min). Sonication washes were repeated with double distilled H<sub>2</sub>O (ddH<sub>2</sub>O), then isopropanol. Wafers were dried and treated with air plasma for 5 min (Henniker Plasma-HPT-100). 100  $\mu$ L of GO solution (0.2 mg mL<sup>-1</sup>) was spin-coated (Laurell WS-650MZ-23NPPB) on wafers at 2500 rpm for 30 s, then set in a desiccator overnight. Flake thickness was characterized using AFM (Asylum MFP-3d, Oxford Instruments, UK), using air tapping mode and data processed with WsxM 4.0 software.<sup>[18]</sup> 40  $\mu$ m  $\times$  40  $\mu$ m from three regions across the wafer were scanned. Lateral flake size was evaluated using scanning electron microscopy (SEM, Zeiss Ultra, accelerating voltage; 10 kV). Flakes were characterized using Raman spectroscopy (inVia, Renishaw model,  $\lambda = 514$  nm, power < 15  $\mu$ W,  $t_{exp} < 10$  s). Raman shift analysis was set between 800 and 1800 cm<sup>-1</sup> and spectra processed using WiRE (Renishaw, UK). GO transmission spectra were measured for oxygen functional groups, using Fourier-transform infrared (FTIR) spectroscopy (Instrument; Nicolet iS5 Software; OMNIC). GO (0.5 mg mL<sup>-1</sup>) was dried in vacuum ( $-1.0$  bar, room temperature) for 72 h prior to FTIR and samples were measured using attenuated total reflectance method.

For GO substrate production, glass coverslips (13 mm diameter, Scientific Laboratory Supplies, UK) were used as a support and comparative platform *in vitro*. Coverslips were cleaned, dried, and plasma-treated using the procedure as outlined for SiO<sub>2</sub> wafers, with the exception of Decon-90:ddH<sub>2</sub>O for the first sonication step rather than acetone. GO solution (80  $\mu$ L, 2 mg mL<sup>-1</sup>) was pipetted onto the coverslip and deposited through spin-coating (4000 rpm, 1 min). Glass and GO substrates were thermally treated at 120 °C for 45 min on an Isotemp hotplate (Fisher Scientific, UK). Substrates were sterilized prior to cell culture use with UV ( $\lambda = 254$  nm, 15 W) for 20 min. GO substrate height and topography were characterized using AFM (three coverslips in total,  $n = 3$ ). Substrates were scratched using fine tweezers to evaluate height discrepancies at the glass–GO boundary (30  $\times$  30  $\mu$ m scan region). The scratch was applied at three random locations on the substrate and four height measurements were taken per scratch region. For topography, four 5  $\times$  5  $\mu$ m regions of glass and GO substrate were imaged. Measurements were carried out using Multi-mode-8 (Bruker, USA) and data processed with WsxM 4.0 software.<sup>[18]</sup> Contact angle of glass and GO substrate were compared for surface wettability, using an optical tensiometer Attension Theta setup (Biolin Scientific, UK). ddH<sub>2</sub>O was

applied using a microsyringe needle ( $0.8 \times 40$  mm, BD micro-lance, UK), with angle recorded at 30 fps. Three samples per group were used, with two droplets per sample. Profiles were fitted using the Young–Laplace model and OneAttention software (Biolin Scientific, UK). Measurements were taken at room temperature and data were expressed as mean  $\pm$  SEM. GO substrate chemical composition was evaluated through XPS. GO solution ( $2 \text{ mg mL}^{-1}$ ) was dropcasted, thermally treated, and sterilized with UV using the procedure outlined for substrate production. Material was dried for 48 h in vacuum. Analysis was done with monochromatic Al  $K\alpha$  source ( $1486.6 \text{ eV}$ ). Spectra were collected at  $20 \text{ eV}$  energy with  $0.5 \text{ eV}$  resolution degrees. Peak fitting for carbon 1s and oxidation degree was achieved using CasaXPS software. Shirley background subtraction was implemented and calibration done at  $284.5 \text{ eV}$ . The C1s peak was deconvoluted using asymmetric pseudo-Voigt line shape for  $sp^2$  graphite component, with symmetric pseudo-Voigt curves for remaining components.<sup>[19]</sup> Component positions were constrained and fixed with FWHM constraints optimized within  $0.7\text{--}2 \text{ eV}$  range.

## 2.2. Human Adipose-Derived Mesenchymal Stromal Cells Harvest and Schwann-Like Adipose Derived Mesenchymal Stromal Cells Stimulation

AD-MSCs were isolated from human tissue biopsies, following procedures approved by the National Research Ethics Committee, UK (NRES 13/SC/0499). Ten patients in total were used, with biopsies harvested from the abdominal site of female patients undergoing reconstructive breast surgery (Age range: 32–64 years). Adipose tissue was separated from skin and fibrous regions and then dissociated mechanically with a razorblade. The tissue was treated with collagenase ( $0.2\% \text{ w/v}$ ) in Hank's balanced salt solution (HBSS) with  $1\% \text{ v/v}$  Penicillin–Streptomycin (P–S), under constant agitation in a water bath for 45 min ( $280 \text{ revs/min}$ ,  $37 \text{ }^\circ\text{C}$ ). Tissue was filtered through a nylon mesh ( $100 \mu\text{m}$ ) and supplemented with  $20 \text{ mL}$  minimum essential medium eagle alpha ( $\alpha\text{MEM}$ ), with  $10\%$  fetal bovine serum (FBS, Labtech, UK),  $1\% \text{ P-S}$ , and  $200 \text{ mM}$  glutamate. This is referred as growth media. Tissue was centrifuged ( $300 \times g$ ,  $10 \text{ min}$ , Instrument; U-32 R, Boeco, Germany) to separate stromal vascular fraction (SVF). The SVF pellet was suspended in  $1 \text{ mL}$  red lysis buffer for  $1 \text{ min}$  and neutralized with growth media exposure ( $15 \text{ mL}$ ). The suspension was centrifuged ( $300 \times g$ ,  $10 \text{ min}$ ), then suspended in growth media. Isolated SVF were cultured in T75 flasks, at  $37 \text{ }^\circ\text{C}$ ,  $5\% \text{ CO}_2$ . Three medium changes were applied weekly. Passaging occurred at  $80\%$  confluency. Cells were classified as AD-MSCs following initial passage. MSCs phenotype was confirmed by surface antigen expression and multipotent differentiation (Figure S1, Supporting Information).<sup>[20]</sup>

For “Schwann-like” AD-MSC (sAD-MSC) stimulation, cells were seeded at  $2 \times 10^5$  cells per T75 at passage 2. Populations were exposed to  $1 \text{ mM}$   $\beta$ -mercaptoethanol for  $24 \text{ h}$  and washed twice with HBSS. Cells were primed with  $35 \text{ ng mL}^{-1}$  all-trans-retinoic acid in growth media over  $72 \text{ h}$ . Stimulation was induced using growth media supplemented with  $5 \text{ ng mL}^{-1}$  platelet-derived growth factor (Peprotech, UK),  $10 \text{ ng mL}^{-1}$  basic fibroblast growth factor (Peprotech, UK),  $14 \text{ mM}$  Forskolin and

$192 \text{ ng mL}^{-1}$  glial growth factor (Acorda Therapeutics, Ardsley, NY, USA). This was classified as maintenance media (MM). Stimulation occurred over  $14 \text{ days}$ . Three MM changes were applied weekly, with passaging at  $80\%$  confluency. Following  $14 \text{ days}$ , cells were classified sAD-MSC. Experiments were carried out using sAD-MSC passage 4–6. Stimulation was confirmed using morphological assessment and immunostaining Schwann markers (Figure S2, Supporting Information).

## 2.3. Schwann-Like Adipose Derived Mesenchymal Stromal Cells Transcriptome Sequence Following Graphene Oxide-Substrate Incubation

sAD-MSCs from four patient-samples ( $N = 4$ ) were used for transcriptome sequencing.  $5 \times 10^4$  cells were plated per glass or GO substrate, in triplicate ( $n = 3$ ). RNA was isolated after  $3 \text{ days}$  incubation, using RNeasy kit, following manufacturer instructions (Qiagen, UK). Concentration and purity were evaluated using QuBit fluorometer (Thermo Fisher) and TapeStation 2200 (Agilent), respectively. Total RNA was submitted to the Genomic Technologies Core Facility and libraries generated using the TruSeq Stranded mRNA assay (Illumina, Inc.) according to the manufacturer's protocol. Briefly, total RNA ( $0.1\text{--}4 \mu\text{g}$ ) was used as input material from which polyadenylated mRNA was purified using poly-T, oligo-attached, and magnetic beads. mRNA was fragmented using divalent cations under elevated temperature and reverse transcribed into first strand cDNA using random primers. Second strand cDNA was then synthesized using DNA polymerase I and RNase H. Following single “A” base addition, adapters were ligated to the cDNA fragments, and the products were purified and enriched by PCR to create the cDNA library. Adapter indices were used to multiplex libraries, which were pooled prior to cluster generation using a cBot instrument. The loaded flow-cell were paired-end sequenced ( $76 + 76$  cycles, plus indices) on an Illumina HiSeq4000 instrument (Illumina, UK). Finally, the output data was demultiplexed (allowing one mismatch) and BCL-to-Fastq conversion was performed with Illumina's bcl2fastq software (version 2.17.1.14).

An average of  $32$  million unique reads was achieved. Unmapped paired-end sequences from Illumina's software sequencer were assessed by FastQC.<sup>[21]</sup> Sequence adapters were removed and reads were quality trimmed using Trimmomatic.<sup>[22]</sup> Reads were mapped against reference human genome (hg38) and counts per gene calculated using annotation from GENCODE-30 (<http://www.encodegenes.org/>) and STAR.<sup>[23]</sup> Normalization, principal component analysis (PCA), and differential expression were calculated with DESeq2.<sup>[24]</sup> Genes achieving adjusted  $p$ -value  $< 0.05$  and  $> 50$  normalized counts were considered significantly different. RNA-seq data has been uploaded in ArrayExpress database (<https://www.ebi.ac.uk/arrayexpress/>) under accession no. E-MTAB-10078.

## 2.4. Schwann-Like Adipose Derived Mesenchymal Stromal Cells Viability Assessment

Three patient-samples in total ( $N = 3$ ) were used to study sAD-MSC viability on GO substrates. Plasma membrane

integrity and metabolic rate was assessed using LIVE/DEAD cytotoxicity kit (Peptrotech, UK) and CellTiter MTS kit (Promega, UK), respectively.  $1 \times 10^4$  sAD-MSCs were seeded per material group, in triplicate ( $n = 3$ ). For cell viability, media was aspirated and cells incubated in  $\alpha$ MEM (no phenol red) with Ethidium homodimer-1 ( $2 \mu\text{g mL}^{-1}$ ) and Calcein-AM ( $0.5 \mu\text{g mL}^{-1}$ ) for 15 min at  $37^\circ\text{C}$ . Cells were imaged via fluorescence microscopy (Olympus GX71, U-RFL-T mercury lamp). Images were blinded and viable cells quantified using ImageJ. Data were expressed as cell viability  $\% \pm \text{SEM}$ , comparing viable numbers to sAD-MSC on glass at day 3 and 7 ( $n = 3$ ). Metabolic activity was assessed through one-step MTS assay. Media was aspirated and cells were washed with phosphate buffer saline (PBS). Groups were exposed to  $\alpha$ MEM (no phenol red) with CellTiter Aqueous One Solution Cell proliferation media (20% v/v) for 90 min at  $37^\circ\text{C}$ . Colorimetric absorbance was recorded at 490 nm (Asys UVM-340 microplate reader). Absorbance data was normalized to sAD-MSC set on glass (day 3). Data were expressed as average  $\pm \text{SEM}$  ( $n = 3$ ). Alongside viability assays, sAD-MSC morphology changes and adhesion on glass and GO substrate were evaluated (Figure S3, Supporting Information).

## 2.5. Quantitative Real-Time Polymerase Chain Reaction

To evaluate neurotrophin gene expression, four patient-samples were used in total ( $N = 4$ ).  $5 \times 10^4$  sAD-MSCs were plated per group, in triplicate ( $n = 3$ ) and RNA was extracted using the QIAGEN kit outlined previously. Neurotrophin expression was evaluated at day 3 and day 7. RNA concentration and purity were determined via ND-100 Nanodrop (Thermo Fisher Scientific). Genes were investigated through quantitative real-time polymerase chain reaction (qRT-PCR). 300 ng of RNA was transcribed using First Strand RT kit following manufacturer's protocol (Qiagen, UK), at  $42^\circ\text{C}$  for 5 min, with addition of DNA elimination buffer.  $3 \text{ ng } \mu\text{L}^{-1}$  per sample used for initial amplification. Gene expression was measured using SYBR Green (Qiagen) and  $\Delta\Delta\text{CT}$  method. The following cycle parameters were used; initiation set at  $95^\circ\text{C}$  for 10 min, amplification over 40 cycles, denaturation at  $95^\circ\text{C}$  for 15 s, annealing at  $55^\circ\text{C}$  for 30 s, and extension at  $72^\circ\text{C}$  over 30 s. Melt curve was performed over 30 min ( $65\text{--}95^\circ\text{C}$  increase at  $1^\circ\text{C min}^{-1}$  increment). Primers used are outlined in **Table 1** (PrimerDesign Ltd., Southampton, UK). Data were expressed as fold change  $\pm \text{SEM}$  ( $n = 4$ ), using 18S rRNA as house-keeping gene. Fold change was normalized for sAD-MSC set on glass (day 3).

**Table 1.** Primer sequence for qRT-PCR.

Gene	Reference	Forward primer	Reverse primer	Size [BP]
18S rRNA	HK-SY-hu	Primer data set in Kit (Reference Outlined).		/
GDNF	NM_00514	GCTCCAGAGACTGCTGTGTAT	TCCTCTTCTTCTCTCTCTCT	128
BDNF	NM_001709	AGGTGGCTCTGGAATGACAT	TGGGATGGTGGGCATAAGT	129
NGF	NM_002506	AGGAGCAAGCGGTCATCAT	GTCTGTGGCGGTGTCTT	102

## 2.6. Neurotrophin Enzyme-Linked Immunosorbent Assay

Neurotrophin secretion from sAD-MSC on glass and GO substrates was assessed using RayBiotech ELISA kits (RayBiotech, UK).  $5 \times 10^4$  cells were plated per group in triplicate ( $n = 3$ ). Supernatant was collected at day 3 and day 7, then snap-frozen in liquid  $\text{N}_2$  and kept at  $-80^\circ\text{C}$  prior to use. For BDNF enzyme-linked immunosorbent assay (ELISA) microplate, the supernatant was applied directly. The same supernatant was concentrated threefold ( $2600 \times \text{g}$ , 45 min) at  $4^\circ\text{C}$  using centrifugal filter units (Amicon 3 kDa molecular weight cut-off, Merck, UK) prior to applying to the GDNF microplate. For NGF secretion, supernatant was concentrated twofold using the same centrifugation parameters as above. Measurements were carried out following manufacturer's protocol. Four patient-samples were used for BDNF and GDNF experiment ( $N = 4$ ), whereas three patient-samples were used for NGF ( $N = 3$ ). Protein concentration was measured through colorimetric absorbance at 450 nm ( $n = 3$ , Asys UVM-340), using each kit's standard curve as reference. Results were plotted as protein production across all patient-samples, using sAD-MSCs incubated on glass (day 3) control. Absolute protein secretion per patient-sample is outlined in Figure S4, Supporting Information.

## 2.7. Neuron Harvest, Schwann-Like Adipose Mesenchymal Stromal Cells Assisted Regeneration, and Neurite Immunostain

Neurons were harvested from Sprague–Dawley rats (250–300 g) following the de Luca (2015) protocol.<sup>[25]</sup> Animals were terminated via cervical dislocation then decapitation. All animals were maintained in accordance with the UK Animals Scientific Procedures Act (1986). Spinal cords were removed, and vertebrate canals cleaved from connective tissue under dissecting microscope to expose dorsal root ganglia (DRG). The DRG segments were transferred to a petri dish (30 mm) and digested in Ham's F12 media ( $37^\circ\text{C}$ , 1.8 mL) mixed with collagenase type IV stock solution (0.125%). Digestion lasted for 1 h at  $37^\circ\text{C}$ , after which DRGs were washed thrice with F12 media. The collagenase digestion procedure was repeated for 45 min. Following the second collagenase exposure and wash, DRGs were submerged in Ham F12 media (1.8 mL), mixed with trypsin (0.25%), and incubated at  $37^\circ\text{C}$  for 30 min. Trypsinized DRGs were neutralized with 1.5 mL F12 (30% FBS), then dissociated mechanically using a Pasteur pipette. The procedure was repeated five times to yield 8–10 mL of tissue, which was filtered through  $70 \mu\text{m}$  nylon mesh (Corning, UK). Neurons were centrifuged ( $160 \times \text{g}$ , 10 min) and suspended in 500  $\mu\text{L}$  F12 media. Cell populations were separated using F12 with 15% bovine serum albumin and



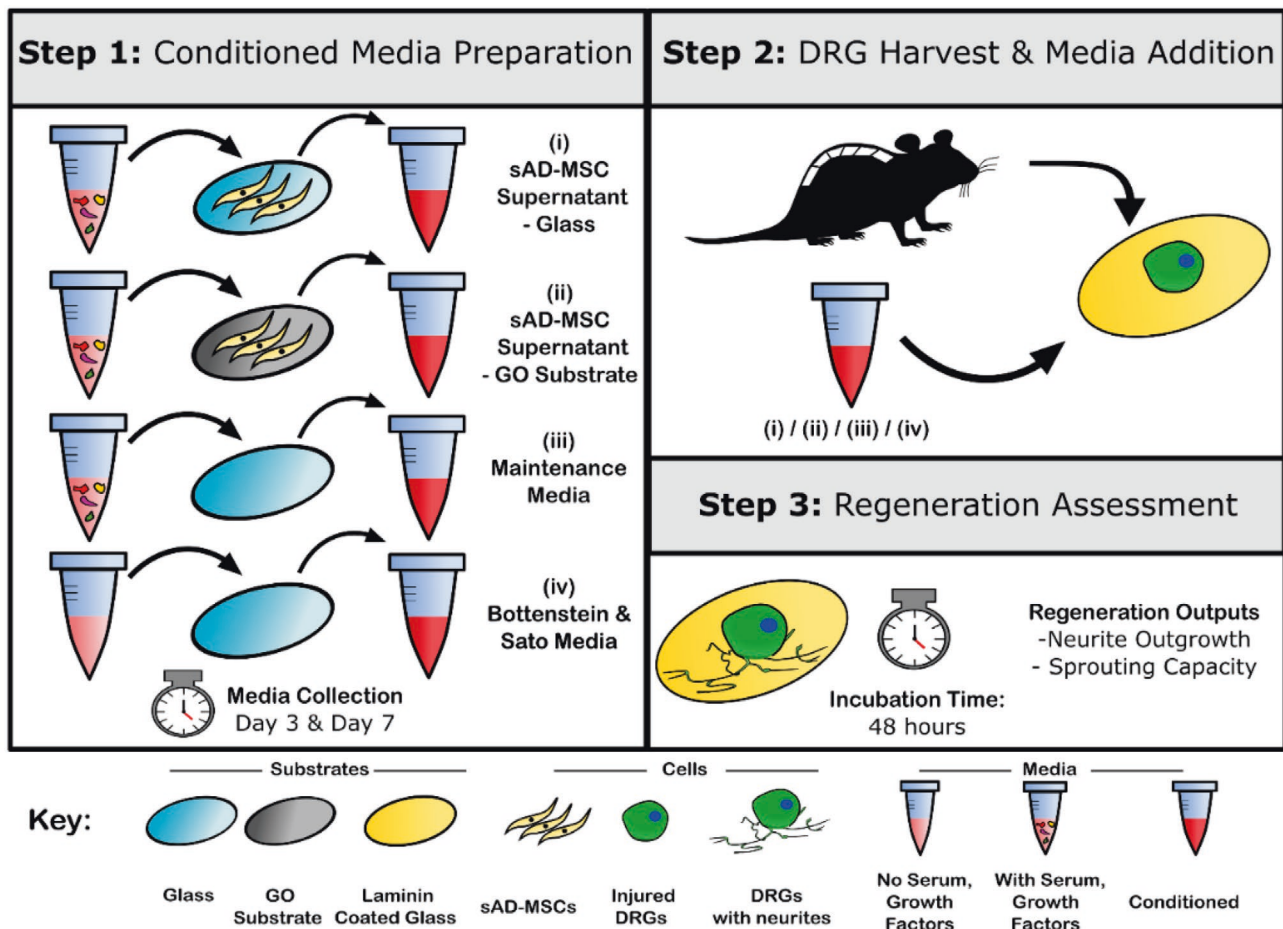


**Figure 1.** Conditioned media culture model. Step 1) Conditioned media collected from sAD-MSC incubated on glass or GO substrates at day 3 and day 7. Maintenance media was used to control sAD-MSC effect, whereas BSM was used to account for growth factor and sera regenerative effects. Step 2) At a similar time, DRGs were harvested from rat and incubated for 24 h. DRGs were exposed to conditioned media for 48 h. Step 3) Regeneration was evaluated through neurite outgrowth and sprouting capacity measurements.

centrifugation ( $300 \times g$ , 10 min). DRG neuron population was plated on laminin-coated glass coverslips for 24 h. Glass coverslips were autoclaved and exposed to poly-lysine for 30 min. Laminin solution ( $10 \mu\text{g mL}^{-1}$ ) was added to each coverslip and incubated for 2 h at  $37^\circ\text{C}$ . Laminin-coated surfaces were washed with PBS. DRG neurons were maintained in Bottenstein and Sato media (BSM) with  $100 \mu\text{L}$  cytosine arabinoside.

Following 24-h attachment in vitro, DRG neurons were supplemented with supernatant originating from sAD-MSC patient-sample ( $N = 1$ ) incubated on GO substrate or glass. An outline of the indirect regeneration model is set in **Figure 1**.  $5 \times 10^4$  sAD-MSCs were plated per group, in triplicate ( $n = 3$ ). The cell supernatant was collected at day 3 or day 7, then snap-frozen prior to use. MM and BSM were prepared as controls for sAD-MSC secretome and growth factor influence, respectively. The MM applied to sAD-MSC and neurons was supplemented with 1% FBS rather than 10% to negate sera recovery effects. Following collection, sAD-MSC supernatant, MM and BSM are referred as conditioned media. DRGs neurons were exposed to conditioned media for 48 h and subsequently fixed in 4% PFA. Neurons were exposed to Triton-X100 (0.2%) for 30 min. DRG

neurons were set in normal goat serum (5:100) for 1 h at room temperature. Neurite outgrowth from DRG neuron populations were assessed using primary  $\beta$ -III Tubulin mouse monoclonal antibodies (1:500, Merck). DRGs were exposed to the antibody for 2 h at room temperature. Samples were washed thrice in PBS and exposed to 488 nm Alexa Fluor-conjugated mouse antibody (1:500, Thermo Scientific). Cells were washed thrice in PBS prior to imaging. Neurite length and sprouting population were evaluated through fluorescent microscopy (Olympus GX71, U-RFL-T mercury lamp). DRG groups were blinded before imaging and imaging per group was done in triplicates ( $n = 3$ ).

## 2.8. Schwann-Like Adipose Derived Mesenchymal Stromal Cells Detachment Evaluation on Graphene Oxide Substrates

To evaluate sAD-MSC detachment in apoptotic conditions, three patient-samples were used ( $N = 3$ ).  $1 \times 10^4$  sAD-MSCs were plated on glass, GO substrate, or fibronectin-coated coverslips, in triplicate ( $n = 3$ ). Fibronectin coverslips were prepared like laminin coatings ( $10 \mu\text{g mL}^{-1}$ ). After 24 h attachment,

cells were exposed to PBS mixture (without  $\text{MgCl}_2/\text{CaCl}_2$ ) for 30 min to induce detachment. To assess viability, PBS was aspirated and cells were incubated with ethidium homodimer-1 ( $2 \mu\text{g mL}^{-1}$ ) and Calcein-AM ( $0.5 \mu\text{g mL}^{-1}$ ) from LIVE/DEAD cytotoxicity kit (Peprotech, UK) for 15 min at  $37^\circ\text{C}$ . Cells were imaged via fluorescence microscopy (Olympus GX71, U-RFL-T mercury lamp). Images were blinded and viable cells, classified with spindle morphology, were quantified using ImageJ. Data were expressed as cell viability  $\% \pm \text{SEM}$ , compared to glass group. For metabolic activity, cells were exposed to DMEM (no phenol red) with 20% v/v CellTiter Aqueous One Solution Cell proliferation media (Promega, UK) for 90 min at  $37^\circ\text{C}$ . Cell numbers were assessed with colorimetric absorbance ( $490 \text{ nm}$ , Asys UVM-340 microplate reader). Data was expressed as absorbance  $\pm \text{SEM}$  ( $n = 3$ ).

## 2.9. Statistical Analysis

Statistical tests were carried out using GraphPad Prism (V7, Graphpad software, La Jolla, CA, USA). Data were expressed as mean  $\pm \text{SEM}$ . Protocols with two experimental groups were evaluated using student's *t*-test, whereas sAD-MSC detachment experiment used ordinary one-way ANOVA. Experiments with

more than two parameters (substrate and timepoint) were compared using two-way ANOVA test followed by Sidak's multiple comparison test. Orders of significance were represented by default *p*-value format set in GraphPad Prism (V7); \**p* < 0.05, \*\**p* < 0.01, \*\*\**p* < 0.001, and \*\*\*\**p* < 0.0001. # indicated statistical significance across timepoints rather than material group. Biological replicates from patient-samples were labeled *N* and experimental replicate was labeled *n*.

## 3. Results

### 3.1. Graphene Oxide Substrate's Physical Characteristics Are Consistent for In Vitro Experiments

Prior to substrate development, the average GO flake thickness (Figure 2A) and lateral size (Figure 2B) were evaluated using AFM and SEM, respectively. Thickness was measured at  $1.5 \pm 0.4 \text{ nm}$ , indicating a predominantly monolayer distribution, with an average lateral size of  $6.7 \pm 2.3 \mu\text{m}$ . Raman spectra (Figure 2C) demonstrate *D*-peak ( $1351 \text{ cm}^{-1}$ ) and *G*-peak ( $1593 \text{ cm}^{-1}$ ) with  $I_D/I_G$  of 0.97. FTIR (Figure 2D) indicates abundant oxygen groups with characteristic O–H, C=O, C–O signals. After material deposition, the GO substrate was evaluated

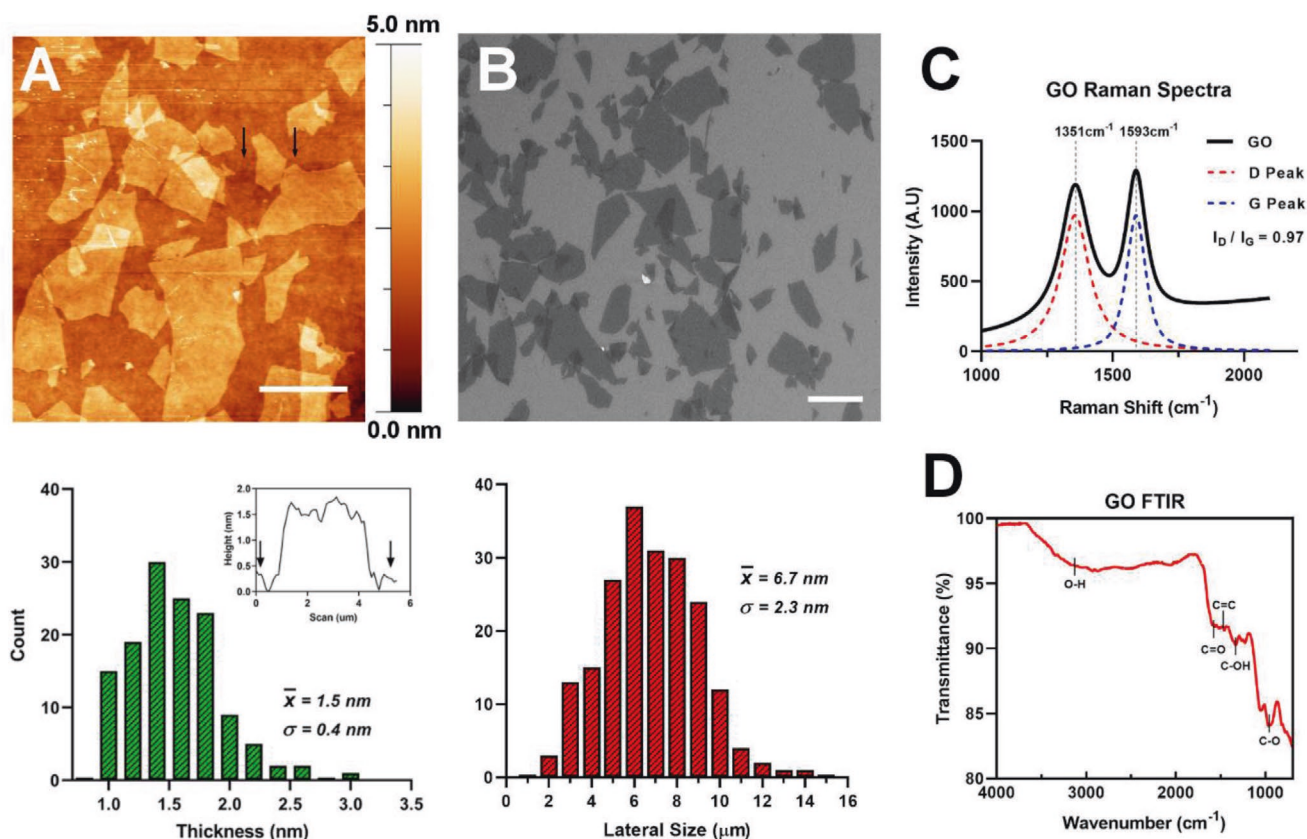


**Figure 2.** Characterization of GO flakes. A) AFM image (top panel) of GO flakes on  $\text{SiO}_2$ . Histogram of total thickness counts (below) outlines a mean height of GO flakes as  $1.5 \pm 0.4 \text{ nm}$ . Arrows represent line profile example of single flake. Distribution suggests majority monolayer in thickness. B) Lateral size of flakes evaluated using SEM. Count (below) indicates average lateral size of  $6.7 \pm 2.3 \mu\text{m}$ . C) Raman spectra of GO flakes indicate  $I_D/I_G$  peak of 0.97 and D) FTIR indicate abundant oxygen functional groups. Scale bars represent  $10 \mu\text{m}$ .

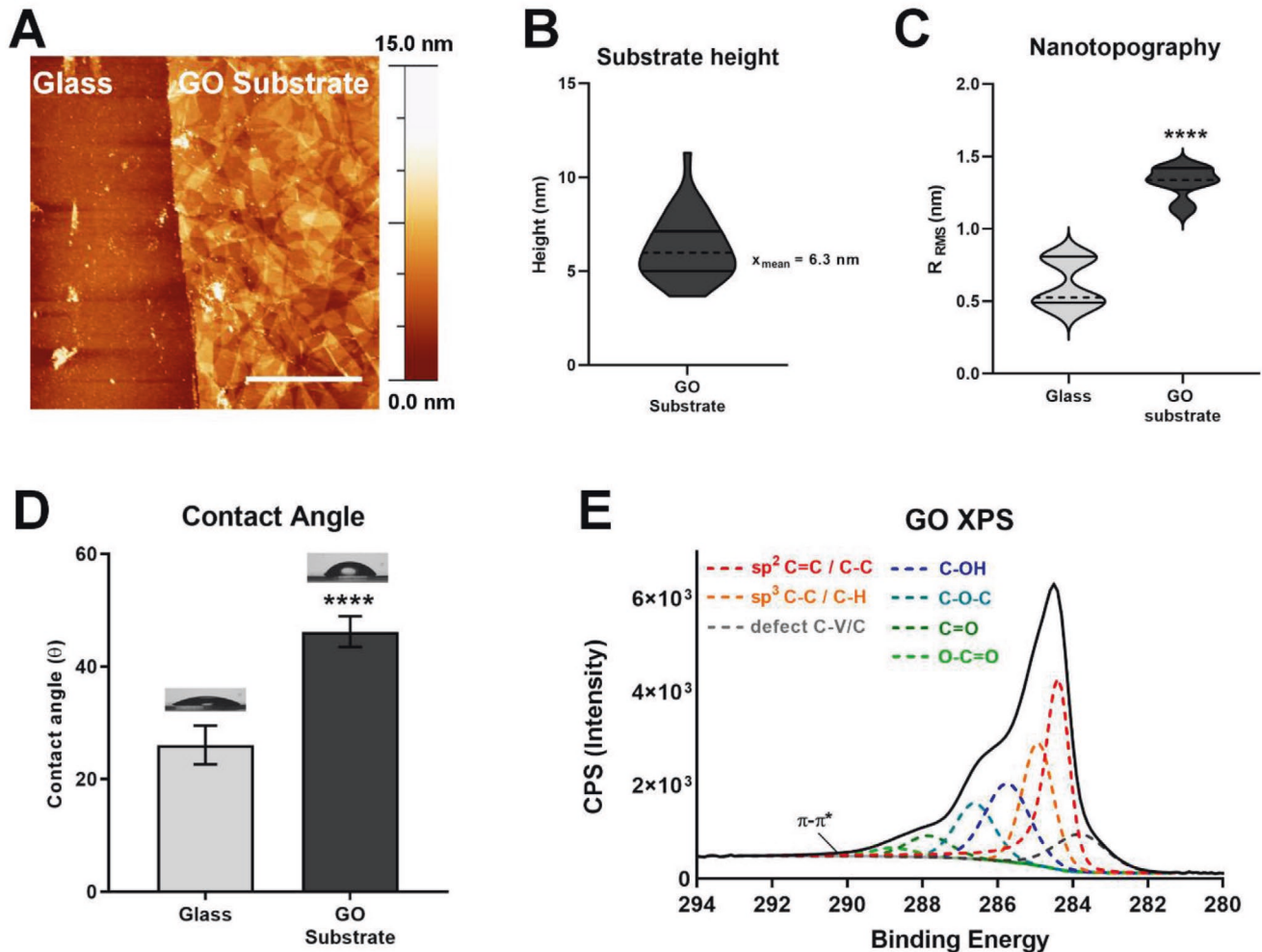


**Figure 3.** Characterization of GO substrate. A) First panel shows the scratch assay exposing the glass support underneath on the left and the GO substrate on the right. Scale bar represents 10  $\mu\text{m}$ . B) Height distribution at the glass–GO boundary following scratch in substrate. Mean height was calculated as  $6.3 \pm 0.3$  nm. C) The nanotopography of the glass and GO substrate. Glass control exhibits lower average RMS for roughness compared to GO substrate ( $0.6 \pm 0.1$  nm vs  $1.3 \pm 0.1$  nm, \*\*\*\* $p < 0.0001$ ). D) Glass control surface is more hydrophilic compared to GO substrate ( $26.1 \pm 3.5^\circ$  vs  $46.2 \pm 2.9^\circ$ ,  $p < 0.0001$ ,  $n = 3$ ). E) XPS spectra following thermal annealing indicates presence of three carbon peaks associated with vacancy defects (283.3 eV),  $\text{sp}^2$  (284.4 eV), and  $\text{sp}^3$  (284.9 eV) hybridization, with  $\pi$ – $\pi^*$  satellite C=C peak detected (290 eV). Oxygen-functionalized carbon peaks attributed to C–OH (285.7 eV), C–O–C (286.6 eV), C=O (287.8 eV), and O–C=O (288.8 eV). C to O ratio was calculated at 2.94.

through AFM (Figure 3A). The average height across the glass–GO boundary was  $6.3 \pm 0.3$  nm, with 75% of height distribution set between 5.1 and 7.2 nm (Figure 3B). The root mean square of GO substrate roughness (Figure 3C) was calculated at  $1.3 \pm 0.1$  nm, which was higher than glass control ( $0.6 \pm 0.1$  nm,  $p < 0.0001$ ). Contact angle measurements (Figure 3D) demonstrated that glass surface was more hydrophilic ( $26.1 \pm 3.5^\circ$ ) compared to the GO substrate ( $46.2 \pm 2.9^\circ$ ,  $n = 3$ ,  $p < 0.0001$ ). The C1s XPS spectrum (Figure 3E) of GO shows presence of oxygen functionalities and defects. Three carbon peaks are centered at 283.8, 284.4, and 284.9 eV, attributed to near vacancy defects,  $\text{sp}^2$ -hybridised aromatic carbon, and  $\text{sp}^3$ -hybridised carbon, respectively.<sup>[26]</sup> Higher energy oxygen-functionalized carbon peaks detected are attributed to phenol (C–OH; 285.7 eV), ether/epoxy (C–O–C; 286.6 eV), ketone (C=O; 287.8 eV), and carboxyl (O–C=O; 288.8 eV). A small  $\pi$ – $\pi^*$

shakeup satellite of the C=C peak was detected at 290 eV. The C to O ratio was calculated at 2.94 from the C1s spectrum.

### 3.2. Differences in Schwann-Like Adipose Derived Mesenchymal Stromal Cells Transcriptome from Graphene Oxide Incubation Is Minimal

sAD-MSC phenotype on GO substrates was evaluated by measuring transcriptome data across four different patient-samples. Variance from each sample was visualized (Figure 4A) through PCA. Plotting the first three principal components (PC) shows sAD-MSC patient-sample origin dictates variability. Material incubation effects are minor in comparison, as sAD-MSC per substrate is clustered per patient-sample. Differential gene expression (Figure 4B) from sAD-MSC incubated on



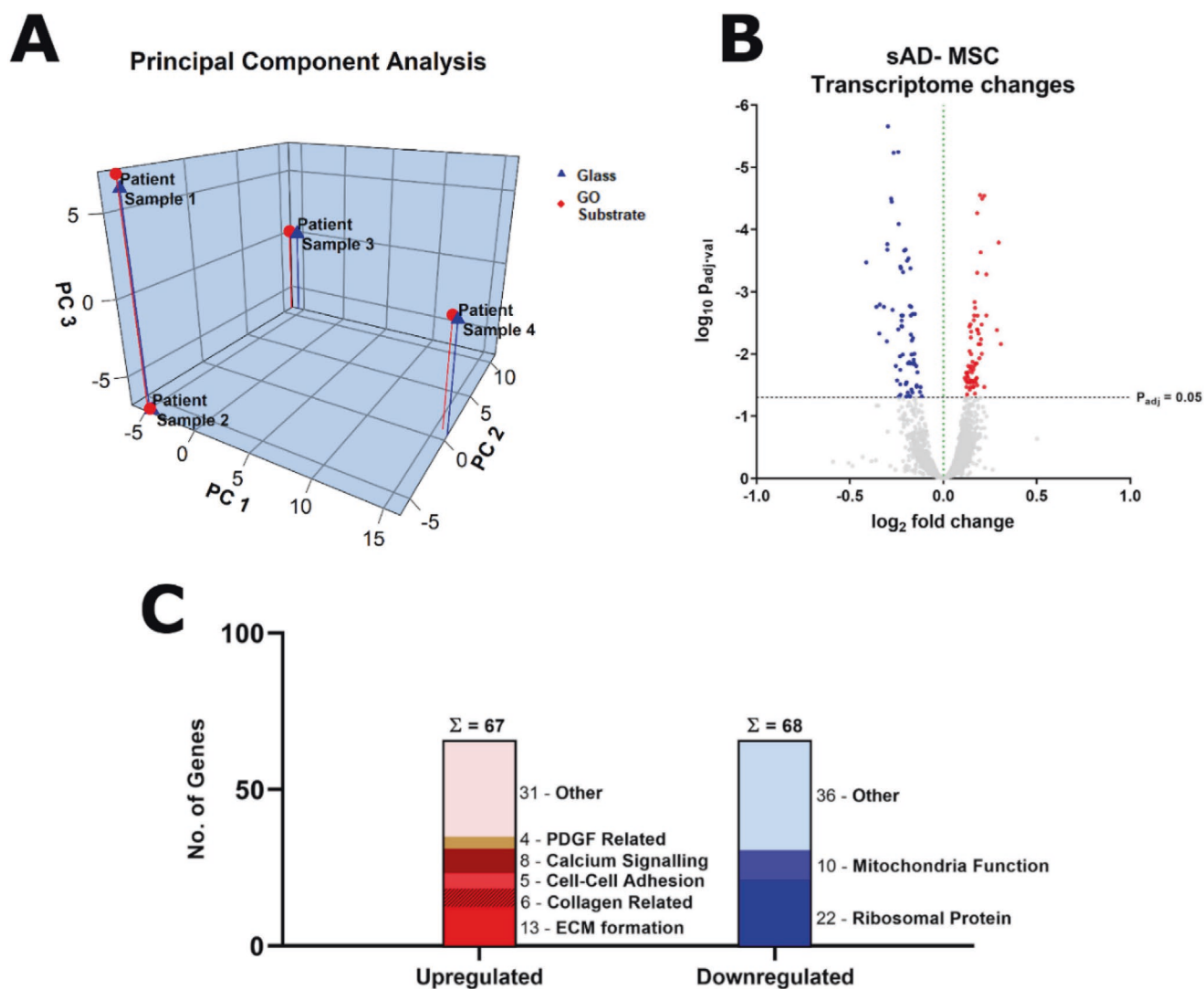


**Figure 4.** GO-substrate dependent transcriptome changes. A) 3D principal component analysis plot produced following RNA sequencing and differential gene expression analysis. Greatest variance observed from sample origin, with glass and GO substrates conditioned-sAD-MSCs still clustered based on patient-sample origin. Patient-sample 4 separated by PC1, patient-sample 3 by PC2, and finally patient-sample 1 and patient-sample 2 are separated through PC 3. Variation from material interaction is minimum in context, as both glass and GO substrate values are in same proximity per sample. B) Volcano plot of upregulated and downregulated genes associated with GO substrate incubation. Total of 135 genes were deemed to be upregulated or downregulated significantly across samples ( $N = 4$ ). Maximum  $\log_2$  fold change for upregulated and downregulated gene corresponds to fold change of 1.24 and 0.75, respectively. C) Upregulated (67) and downregulated (68) genes were grouped. Largest group of upregulated groups include genes associated with ECM formation. Largest group of downregulated groups include genes associated with ribosomal proteins.

GO substrate was plotted for fold change and adjusted  $p$ -value ( $p_{adj} < 0.05$ ) against glass sAD-MSCs genome. A total of 135 genes were significantly altered; 67 genes were upregulated and 68 genes were downregulated. Genes classified as significantly different were grouped (Figure 4C). A proportion of genes upregulated (19) were associated with ECM formation, six of which were collagen related. Other groups include cell-cell adhesion genes (5), one calcium signaling (8), and PDGF-related signaling (4). Downregulated groups included genes with impact on protein synthesis (ribosomal proteins, 22) and genes associated with mitochondrial function (10). The full list of genes affected and the evidence of GO material effects are

outlined in Table S1 and Figure S5, Supporting Information, respectively.

### 3.3. Cell Viability on Graphene Oxide and Control Are Comparable but Metabolic Activity Decreases at Day 3

To evaluate downregulated gene effects and confirm GO as suitable sAD-MSCs substrates, cell viability and metabolism were evaluated using LIVE/DEAD and MTS assays, respectively. sAD-MSCs on glass (Figure 5A) and GO substrates (Figure 5B) were compared via LIVE/DEAD assay at day 3 and day 7. The number



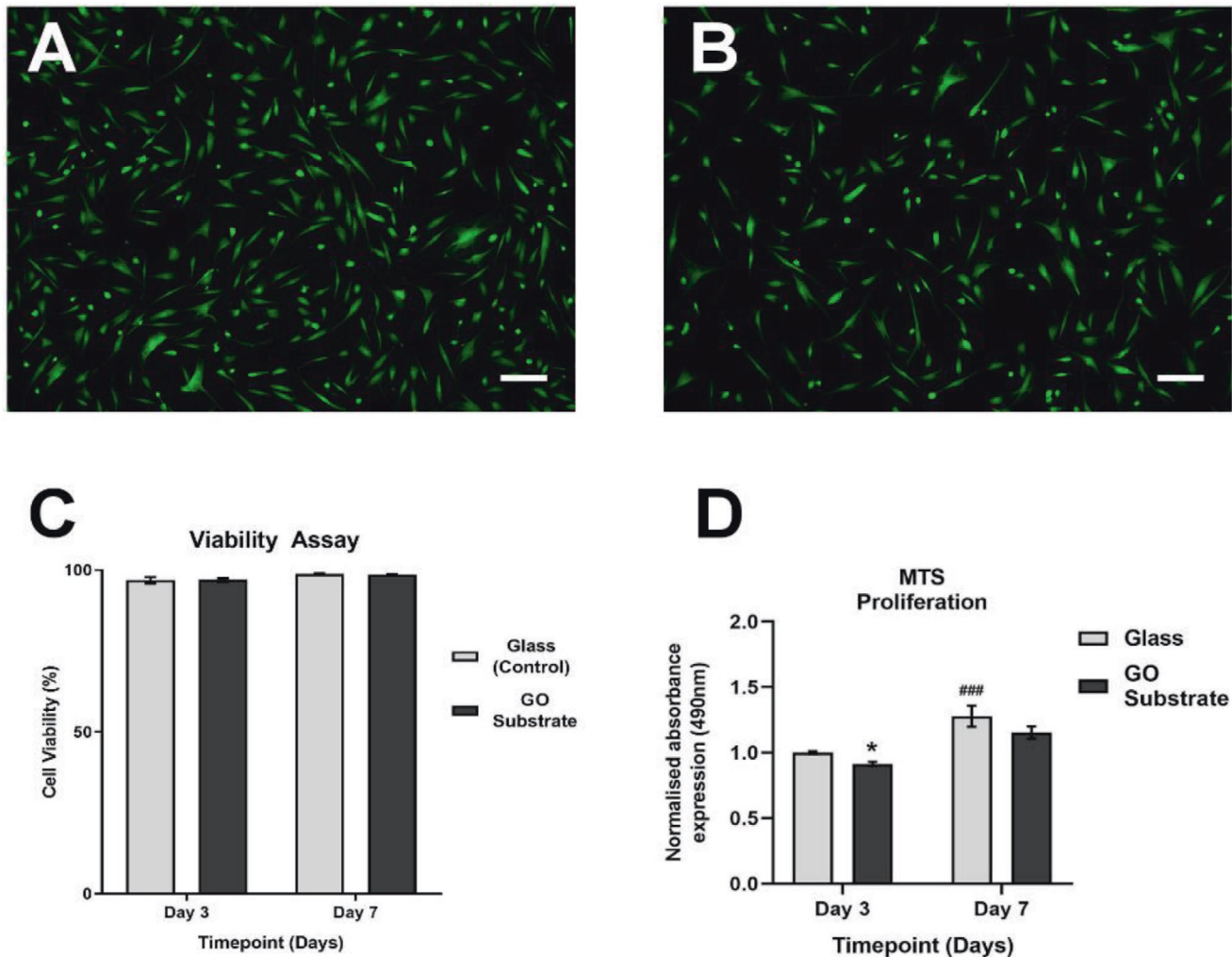


**Figure 5.** sAD-MSC viability on glass and GO substrate. A) Image of live cells on day 3 on glass structure and B) GO substrate. C) Viable sAD-MSC calculated show no difference between glass and GO substrate on day 3 ( $96.8 \pm 1.0$  vs  $96.9 \pm 0.3$ ,  $p = ns$ ,  $n = 3$ ) and day 7 ( $98.7 \pm 0.5$  vs  $98.5 \pm 0.5$ ,  $p = ns$ ,  $n = 3$ ). D) Cell metabolic activity indicates lower absorbance at day 3 between sAD-MSC on GO substrate compared to glass ( $1.000 \pm 0.01$  vs  $0.88 \pm 0.02$ ,  $*p < 0.05$ ,  $n = 3$ ). At day 7, sAD-MSC absorbance on glass was significant ( $1.28 \pm 0.16$ ,  $###p < 0.001$ ,  $n = 3$ ) but sAD-MSC proliferation on GO substrate ( $1.15 \pm 0.05$ ) saw no difference compared to glass day 3. No difference was observed in sAD-MSC activity across materials at day 7 ( $1.28 \pm 0.16$  vs  $1.15 \pm 0.08$ ,  $p = ns$ ,  $n = 3$ ). Absorbance value from sAD-MSC on glass at day 3 used for normalization. Number of patients  $N = 3$ . Data expressed as mean  $\pm$  SEM. \* indicates statistical difference within timepoints, and # indicates statistical difference across timepoints.

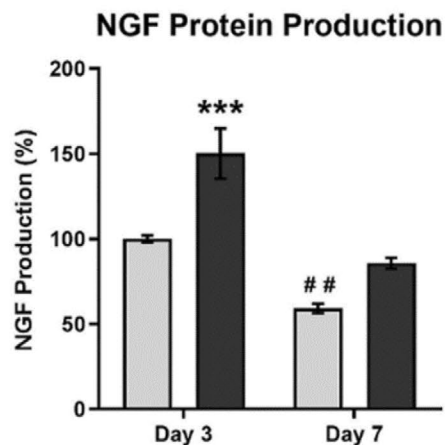
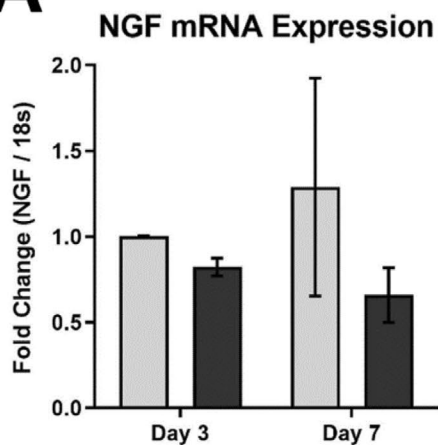
of viable cells on glass and GO substrate were similar at day 3 ( $96.8 \pm 1.0\%$  vs  $96.5 \pm 0.5\%$ ) and day 7 ( $98.7 \pm 0.5$  vs  $98.5 \pm 0.5\%$ ). MTS assay (Figure 5D) demonstrates lower normalized absorbance at day 3 from sAD-MSC on GO substrate ( $0.88 \pm 0.02$ ,  $p < 0.05$ ) compared to control glass population ( $1.00 \pm 0.01$ ). sAD-MSC metabolic activity on glass increased at day 7 ( $1.28 \pm 0.16$ ,  $p < 0.001$ ). Lower absorbance from sAD-MSC on GO substrate was not significant at day 7 ( $1.28 \pm 0.16$  vs  $1.15 \pm 0.08$ ).

### 3.4. Schwann-Like Adipose Derived Mesenchymal Stromal Cells on Graphene Oxide Substrates Increase Nerve Growth Factor and Glial-Derived Neurotrophic Factor Protein Secretion

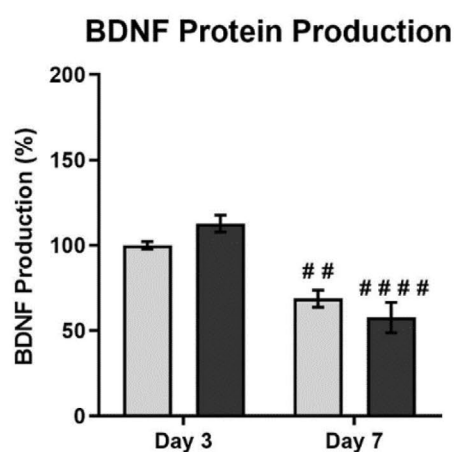
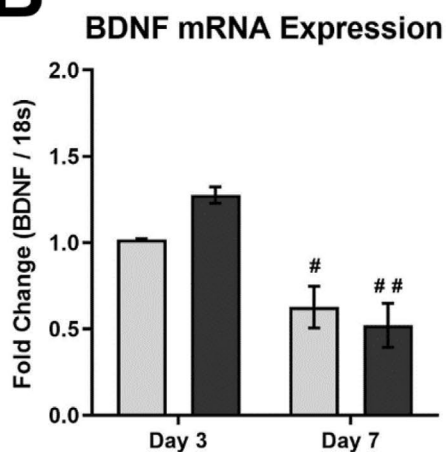
To evaluate sAD-MSC stimulation, NGF, BDNF, and GDNF gene expression was examined using qRT-PCR, and protein

secretion evaluated with ELISA. “Schwann-like” cell regression was monitored at day 7, using sAD-MSC on glass from day 3 as control. NGF gene expression (Figure 6A) from sAD-MSC on glass and GO substrates was similar at day 3 (GO sub:  $0.82 \pm 0.05$ ) and day 7 (glass:  $1.29 \pm 0.64$  vs GO sub:  $0.66 \pm 0.16$ ). sAD-MSC NGF production across patients increased from the GO substrate group at day 3 ( $150 \pm 21.1\%$ ,  $p < 0.001$ ). Compared to control, NGF protein production declined at day 7 from sAD-MSC on glass ( $59.2 \pm 1.9\%$ ,  $p < 0.01$ ) and no significant difference was observed from sAD-MSCs on GO substrate ( $85.8 \pm 2.7\%$ ). BDNF gene expression (Figure 6B) at day 3 for sAD-MSC on GO substrate and glass was similar. At day 7, sAD-MSC BDNF gene expression lowered (glass:  $0.63 \pm 0.12$ ,  $p < 0.05$ ; GO sub:  $0.52 \pm 0.13$ ,  $p < 0.01$ ). No difference in BDNF protein production was observed from sAD-MSC population on glass and GO substrates at day 3 ( $114.1 \pm 10.2\%$ ,

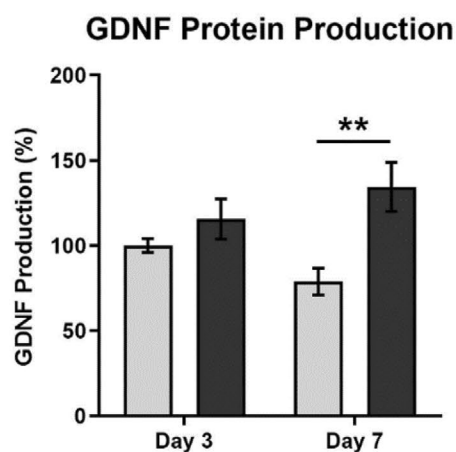
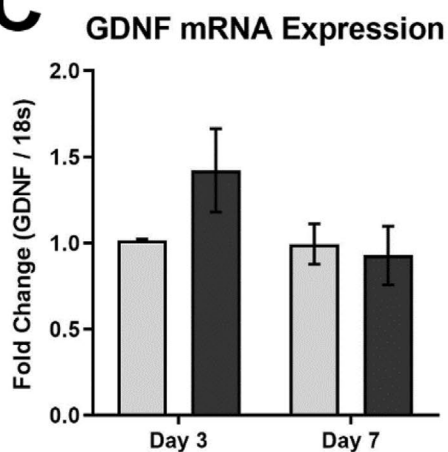
**A**



**B**



**C**



$p = ns$ ) whilst secretion declined at day 7 from sAD-MSC on glass ( $65.8 \pm 10.0\%$ ,  $p < 0.01$ ) and GO substrate ( $53.7 \pm 18.6\%$ ,  $p < 0.0001$ ). GDNF gene expression (Figure 6C) from sAD-MSC on GO substrate at day 3 ( $1.42 \pm 0.24$ ,  $p = ns$ ) was comparable to control. By day 7, no change in sAD-MSCs GDNF expression on glass ( $0.99 \pm 0.12$ ,  $p = ns$ ) or GO substrate ( $0.93 \pm 0.13$ ,  $p = ns$ ) was observed. Protein production for GDNF from sAD-MSC on GO substrate was similar to control ( $117.0 \pm 20.1\%$ ,  $p = ns$ ) at day 3. Then at day 7, a significant difference was observed between sAD-MSC at day 7, dependent on material incubation (glass;  $77.7 \pm 12.6\%$  vs GO sub;  $137.6 \pm 25.8\%$ ,  $p < 0.01$ ).

### 3.5. Dorsal Root Ganglia Recovery Using Culture Media Unaffected from Graphene Oxide Substrate Secretome Changes

In vitro PNI models were evaluated to assess whether differences in NGF and GDNF protein secretion from sAD-MSCs on GO substrates improved regenerative outcomes. Conditioned media harvested from day 3 (Figure 7A) and day 7 (Figure 7B) were supplemented to DRG neurons. Populations exposed to sAD-MSC supernatant or MM from either timepoints demonstrated increased sprouting and neurite outgrowth compared to DRGs maintained in BSM. The average neurite length was measured with supernatant from sAD-MSCs on glass set as the control at each respective timepoint (Figure 7C). sAD-MSC conditioned media on GO substrates did not enhance neurite outgrowth at either timepoint compared to control (day 3:  $161.5 \pm 3.4 \mu\text{m}$ , day 7:  $181.3 \pm 8.7 \mu\text{m}$ ). MM extracted at day 3 resulted in a lower average neurite length, but not at day 7 (day 3:  $123.3 \pm 5.8 \mu\text{m}$ ,  $p < 0.001$ , day 7:  $150.7 \pm 7.1 \mu\text{m}$ ,  $p = 0.1053$ ). DRGs supplemented with BSM at both timepoints exhibited shorter neurites (day 3:  $110.4 \pm 4.2 \mu\text{m}$ ,  $p < 0.0001$ ; and day 7:  $79.2 \pm 11.6 \mu\text{m}$ ,  $p < 0.0001$ ). DRG sprouting was measured using neurons exposed to conditioned media from sAD-MSC on glass as control (Figure 7D). DRG neurons exposed to sAD-MSC conditioned media on GO substrates at day 3 exhibited sprouting capacity similar to control group ( $77.8 \pm 2.1\%$ ), whereas sprouting from DRG neurons supplemented with MM and BSM lowered (MM:  $58.2 \pm 1.4\%$ ,  $p < 0.05$ ; BSM:  $22.6 \pm 3.8\%$ ,  $p < 0.0001$ ). Sprouting from sAD-MSC day-7 conditioned media from glass and GO substrate group were comparable ( $65.7 \pm 2.2\%$  vs  $72.9 \pm 3.3\%$ ). No difference was observed in sprouting from DRG neurons exposed

to day-7 MM ( $67.4 \pm 0.6\%$ ). BSM-supplemented DRG neurons at day 7 exhibited lower sprouting capacity ( $31.9 \pm 5.2\%$ ,  $p < 0.0001$ ).

### 3.6. Cell Viability Enhanced on Graphene Oxide Substrates Compared to Glass After Apoptotic Conditions

Retention of sAD-MSC on GO substrates under apoptotic conditions in vitro was tested using PBS exposure. Fluorescent images demonstrate low numbers of spindle cells on glass substrate following PBS exposure, with majority rounded (Figure 8A). The sAD-MSC population on GO substrates (Figure 8B) were less rounded and a greater number of spindle cells was present. sAD-MSC on fibronectin surface primarily maintained the spindle shape (Figure 8C). A count of viable spindle cells normalized to glass population numbers (Figure 8D), indicate that higher number of viable cells on GO substrates was present ( $2.1 \pm 0.1$ ,  $p < 0.0001$ ). The highest proportion of viable sAD-MSC cells was present on fibronectin ( $5.7 \pm 2.7$ ,  $p < 0.0001$ ). Cell numbers were compared with MTS metabolic activity assay following PBS exposure (Figure 8E). sAD-MSC plated on glass had the lowest absorbance ( $0.095 \pm 0.007$ ). sAD-MSC on GO substrates had higher absorption ( $0.221 \pm 0.010$ ,  $p < 0.0001$ ). sAD-MSC on fibronectin demonstrated highest cell absorbance ( $0.446 \pm 0.105$ ,  $p < 0.05$ ).

## 4. Discussion

We evaluated the suitability of GO substrates as a biomaterial intervention for severe PNI to support and maintain human sAD-MSC. This cell population is dependent on biochemical stimulation; therefore alternative strategies are required for clinical translation. We identified that GO substrates triggered only minor changes in sAD-MSC transcriptome and metabolic activity but increased NGF and GDNF protein secretion which did not translate to improved neuronal regeneration in an indirect in vitro model. Additionally, sAD-MSC viability was enhanced on GO substrates under apoptotic conditions.

GO flakes were characterized prior to substrate production, measuring an average lateral size of 5–6  $\mu\text{m}$  and near monolayer distribution (Figure 2). Microsized GO flake solution was chosen as it shows greater AD-MSC proliferation

**Figure 6.** sAD-MSC neurotrophin expression. A) NGF gene expression from sAD-MSC at day 3 was  $0.82 \pm 0.05$  ( $p = ns$ ,  $n = 4$ ) on GO substrates compared to glass control. At day 7, sAD-MSC NGF expression on glass ( $1.29 \pm 0.64$ ,  $p = ns$ ,  $n = 4$ ) and GO substrate ( $0.66 \pm 0.16$ ,  $p = ns$ ,  $n = 4$ ) were comparable to day 3 control. NGF protein production from sAD-MSC on GO substrates was higher than glass group at day 3 ( $150 \pm 21.1\%$ ,  $***p < 0.001$ ,  $n = 3$ ). After 7 days, sAD-MSC on glass produced less NGF compared to control ( $59.2 \pm 1.9\%$ ,  $##p < 0.01$ ,  $n = 3$ ), but no decrease was observed from sAD-MSC on GO substrates ( $85.8 \pm 2.7$ ,  $p = ns$ ,  $n = 3$ ). B) BDNF gene expression of sAD-MSC on glass and GO substrates at day 3 were comparable ( $1.28 \pm 0.05$ ,  $p = ns$ ,  $n = 3$ ). At day 7, BDNF gene expression decreased for sAD-MSC incubated on glass ( $0.63 \pm 0.12$ ,  $#p < 0.05$ ,  $n = 4$ ) and on GO substrates ( $0.52 \pm 0.13$ ,  $##p < 0.01$ ,  $n = 4$ ) compared to control. BDNF production from sAD-MSC on GO substrates was similar to glass group ( $114.1 \pm 10.2\%$ ,  $p = ns$ ,  $n = 3$ ), but levels decreased from sAD-MSC population on glass (Glass;  $65.8 \pm 10.0$ ,  $##p < 0.01$ ,  $n = 3$ ) and GO Substrate ( $53.7 \pm 18.6\%$ ,  $####p < 0.0001$ ,  $n = 3$ ) at day 7. C) sAD-MSC on GO substrates exhibit GDNF gene expression at day 3 comparable to glass control ( $1.42 \pm 0.24$ ,  $p = ns$ ,  $n = 4$ ). GDNF expression was not significantly different from sAD-MSC on glass ( $0.99 \pm 0.12$ ,  $p = ns$ ,  $n = 4$ ) or GO substrate ( $0.93 \pm 0.13$ ,  $p = ns$ ,  $n = 4$ ) at day 7. GDNF protein production from sAD-MSC on GO substrate was similar to glass control ( $117.0 \pm 20.1\%$ ,  $p = ns$ ,  $n = 3$ ). Compared to control group, no significant different in GDNF production was measured from day 7 sAD-MSC population from either material groups, but significantly less GDNF was produced between sAD-MSC on glass substrate compared to sAD-MSC on GO substrates at day 7 ( $77.7 \pm 12.6\%$  vs  $137.6 \pm 25.8\%$ ,  $**p < 0.01$ ,  $n = 3$ ). \* indicates statistical difference within timepoints, and # indicates statistical difference across timepoints.

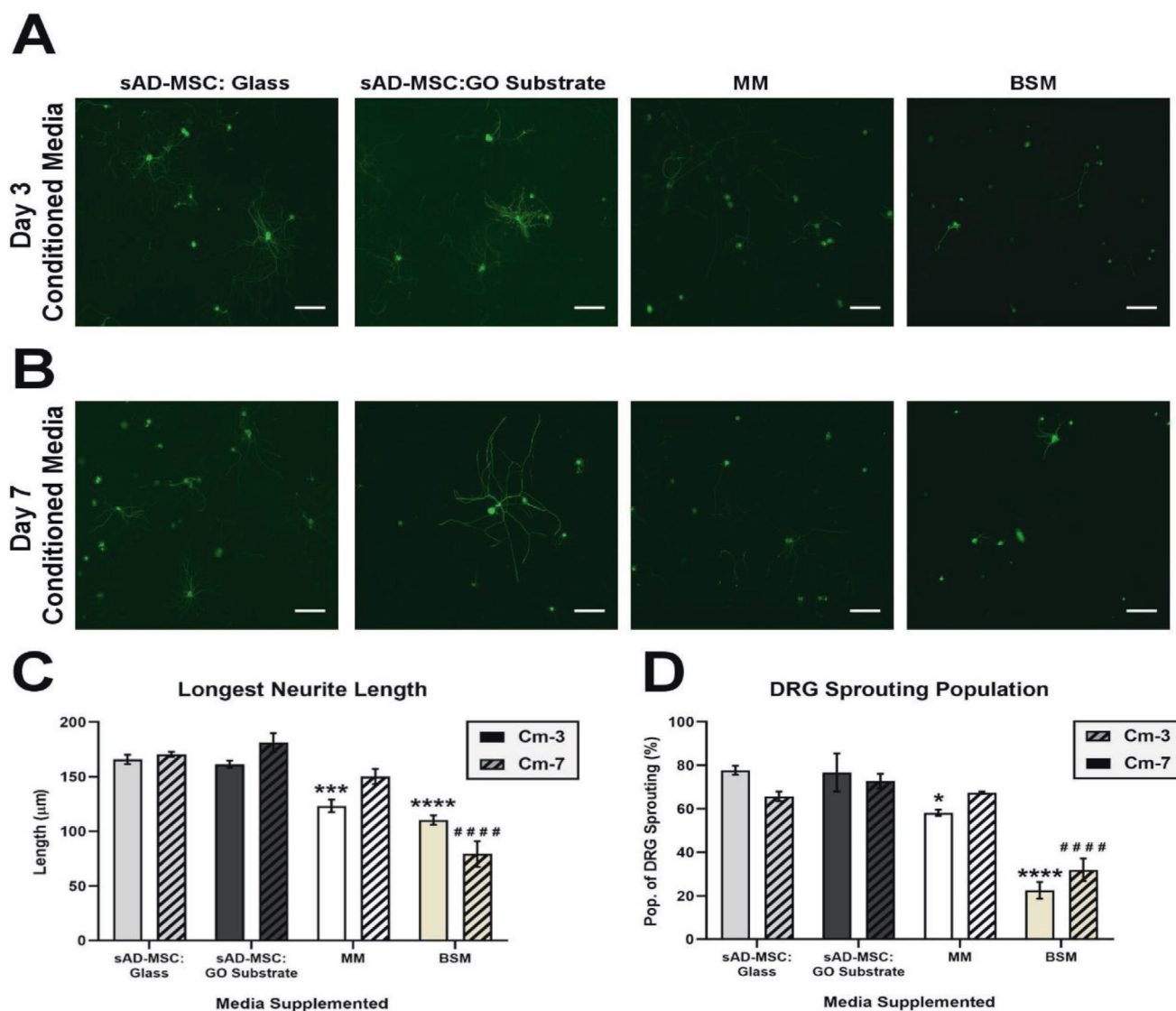


**Figure 7.** Indirect regeneration of DRG neurons. Images of neurite outgrowth from DRG neurons exposed to sAD-MSC supernatant from glass or GO substrate, the maintenance media (MM), or Bottenstein and Sato media (BSM). Media harvested for DRG regeneration referred as conditioned media (Cm). DRG neurons were exposed to conditioned media harvested from A) day 3 (Cm-3) and B) day 7 (Cm-7). Scale bars represent 100 µm. C) Longest neurite observed from DRGs following Cm-3 and Cm-7 exposure, using the DRG group exposed to sAD-MSC from glass' conditioned media as control at each respective timepoint. Compared to glass control ( $165.9 \pm 4.3 \mu\text{m}$ ,  $n = 3$ ), no difference in the longest neurite length from DRG neurons supplemented with sAD-MSC:GO substrate Cm-3 ( $161.5 \pm 3.4 \mu\text{m}$ ,  $p = \text{ns}$ ,  $n = 3$ ) was observed. Both groups exhibited longer neurites than DRG neurons exposed to MM Cm-3 ( $123.3 \pm 5.8 \mu\text{m}$ ,  $***p < 0.001$ ,  $n = 3$ ) and BSM Cm-3 ( $110.4 \pm 4.2 \mu\text{m}$ ,  $****p < 0.0001$ ,  $n = 3$ ). No difference was observed in longest neurite length for DRG neurons supplemented with sAD-MSC:GO substrate Cm-7 ( $181.3 \pm 8.7 \mu\text{m}$ ,  $p = \text{ns}$ ,  $n = 3$ ) compared to glass control ( $170.6 \pm 2.2 \mu\text{m}$ ,  $n = 3$ ). The MM Cm-7 was similarly comparable to control ( $150.7 \pm 7.1 \mu\text{m}$ ). Negative control BSM group demonstrated significantly shorter neurite length ( $79.2 \pm 11.6 \mu\text{m}$ ,  $####p < 0.0001$ ,  $n = 3$ ). D) Sprouting population of DRG neurons from Cm-3 and Cm-7 exposure using sAD-MSC on glass' Cm as control per corresponding timepoint. The sprouting capacity of DRGs supplemented with sAD-MSC:GO substrate' Cm-3 ( $77.8 \pm 2.1\%$ ,  $p = \text{ns}$ ,  $n = 3$ ) was comparable to control ( $76.7 \pm 8.7\%$ ,  $n = 3$ ). Number of sprouting populations of DRG neurons with MM Cm3 ( $58.2 \pm 1.4\%$ ,  $*p < 0.05$ ,  $n = 3$ ) and BSM Cm-3 ( $22.6 \pm 3.8\%$ ,  $****p < 0.0001$ ,  $n = 3$ ) were lower. Cm-7 sAD:GO substrate group of DRG neurons ( $72.9 \pm 3.3\%$ ,  $p = \text{ns}$ ,  $n = 3$ ) were similar to glass control ( $65.7 \pm 2.2\%$ ,  $n = 3$ ), and no difference was observed in DRG sprouting from group exposed to MM Cm-7 ( $67.4 \pm 0.6\%$ ,  $p = \text{ns}$ ). The DRG population exposed to BSM Cm-7 exhibit significantly lower sprouting capacity to control ( $31.9 \pm 5.2\%$ ,  $####p < 0.0001$ ,  $n = 3$ ). \* indicates statistical significance in Cm-3 experiment and # indicates statistical significance in Cm-7 experiments.

and spreading compared to surfaces coated with nano-sized GO flakes.<sup>[27]</sup> Physical parameters of the GO substrate (Figure 3B,C) included a substrate height of 4–11 nm, with a surface roughness ( $R_{\text{RMS}}$ ) between 1–2 nm<sup>2</sup>. Deposition of the

GO substrate changed the surface's wettability, making the surface more hydrophobic than glass control (Figure 3D). GO substrates have been demonstrated to promote MSC membrane-cytoskeletal protein expression such as vinculin, resulting in



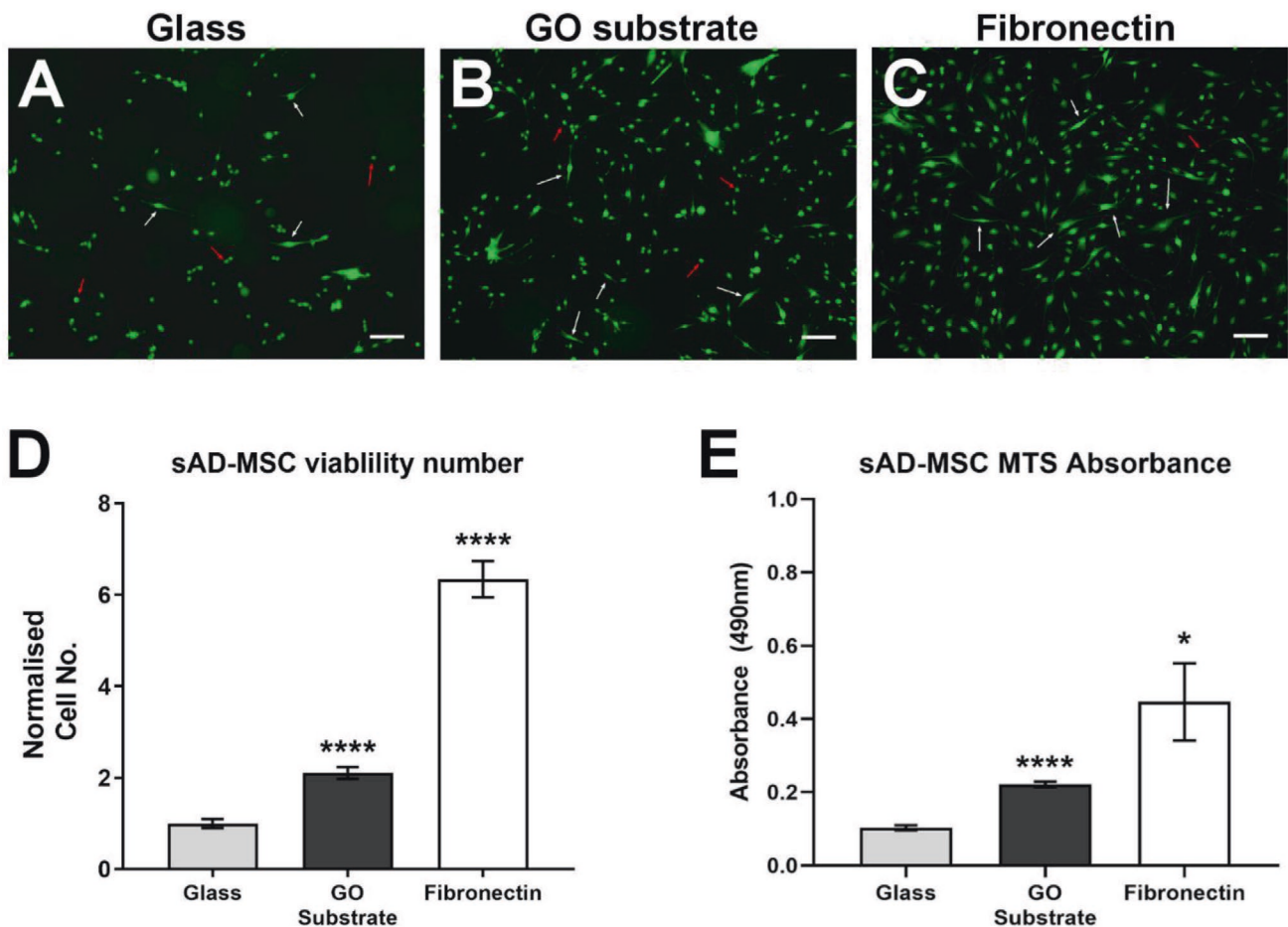


**Figure 8.** sAD-MSC survival in apoptotic conditions. sAD-MSC phenotype and distribution after 30 min PBS exposure on A) glass, B) GO substrate, and C) fibronectin. White arrows indicate cells classified as viable based on spindle morphology. Red arrows indicate rounded cells, classified as non-viable (damaged). Glass control group demonstrated low proportions of viable cells compared to GO substrate. Positive control fibronectin sAD-MSC group have high sAD-MSC viability following PBS exposure. D) Quantification of cell viability based from LIVE/DEAD assay, normalized to glass control. Number of viable sAD-MSC cells observed on GO substrate was  $2.1 \pm 0.1$  greater than glass control ( $****p < 0.0001$ ,  $n = 3$ ). Fibronectin-incubated sAD-MSC exhibited highest proportion of viable cells compared to control ( $5.7 \pm 2.7$ ,  $****p < 0.0001$ ,  $n = 3$ ). E) Cell numbers assessed through MTS assay. sAD-MSCs on glass substrate following PBS exposure had lowest absorbance ( $0.095 \pm 0.007$ ). sAD-MSC on GO substrates demonstrated higher absorbance levels ( $0.221 \pm 0.010$ ,  $****p < 0.0001$ ,  $n = 3$ ). Cells incubated on fibronectin demonstrates significantly higher absorbance levels following PBS exposure ( $0.446 \pm 0.105$ ,  $*p < 0.05$ ,  $n = 3$ ). Scale bar represents 100  $\mu\text{m}$ .

increased focal adhesion points and cytoskeletal strain.<sup>[28]</sup> We saw no changes in sAD-MSC focal adhesion points or vinculin expression after 3 days (see Figure S3, Supporting Information), indicating our GO substrate's topographical features did not substantially affect sAD-MSC adhesion. The XPS spectrum indicated a mildly reduced GO substrate with a 2.94 carbon to oxygen ratio (Figure 3E). Compared to glass surfaces, mildly reduced GO substrates can increase serum and growth factor protein adsorption such as FBS, thereby accelerating cellular attachment.<sup>[29]</sup>

Our harvest, stimulation, and incubation methodology mimics autologous clinical strategies; therefore our results highlight the expected and inherent variability between individual human AD-MSC patient-samples. Biological variance such as age, body-mass index, drug exposure, and ethnicity are parameters that influence AD-MSC viability, proliferation, and differentiation capacity in vitro.<sup>[30,31]</sup> We compared the

transcriptome of sAD-MSC cultured on GO to glass to identify any changes in response attributable to the physicochemical properties of GO. The PCA indicated that patient origin had a far greater impact on sample variance (Figure 4A), with only subtle changes associated with GO substrate incubation (see Figure S5, Supporting Information). Only 135 genes changed significantly across four patients with the greatest upregulated and downregulated fold change being 1.24 and 0.75, respectively (Figure 4B); although among those it is important to note upregulation of several ECM- and collagen-related genes. Tang et al. assessed transcriptome changes from murine neural stem cells on graphene substrates, reporting over 250 upregulated genes and 500 downregulated genes with  $>|2|$  fold-change compared to TCP, with bioinformatic work suggesting stimulated neural differentiation.<sup>[32]</sup> By comparison, our GO substrates were relatively inert which is advantageous as it avoids promotion of undesirable canonical pathways whilst maintaining

viability (Figure 5). Furthermore, our GO interface has capability for highly specific functionalization which could induce targeted MSC differentiation.

The current stimulation strategy to achieve sAD-MSC depends upon a biochemical cocktail, but this phenotype is lost rapidly after withdrawal of stimulation.<sup>[8,33–35]</sup> The first 7 days within the peripheral nerve regeneration environment is crucial for Schwann cell/macrophage recruitment and the initiation of neural growth, therefore sAD-MSC should maintain their stimulated state to be therapeutically feasible.<sup>[1,36]</sup> In order to evaluate early GO substrate effects on sAD-MSCs following withdrawal of stimulation, we monitored NGF, BDNF, and GDNF gene and protein expression over a 7-day period and compared to a glass substrate. Neurotrophin gene expression did not alter substantially; whilst secreted protein levels of NGF were increased at day 3 and of GDNF at day 7 on GO (Figure 6). This observation suggests that GO increases neurotrophin expression in sAD-MSC after removal from biochemical stimulation which would be an exciting adjunct to cell therapy intervention for PNI. This is in keeping with previous work seeking to boost the neurotrophin response of sAD-MSC with external electrical stimulus applied to graphene materials *in vitro*<sup>[37]</sup> and on GO-coated fibers promoting SC transition to a myelinating phenotype.<sup>[13]</sup> Our GO platform compares favorably because higher neurotrophin secretion was observed across human MSC cell populations without need for external stimulus and minimal sAD-MSC genotype influence.

Next, we focused on whether this increase in neurotrophin secretion improved regeneration in injured DRG neurons *in vitro* subject to conditioned media. NGF is a key component in axonal regeneration and sprouting of primary sensory neurons, whereas GDNF affects a subpopulation of isolectin IB4<sup>+</sup> unmyelinated neurons.<sup>[38,39]</sup> Although our model demonstrated no significant changes in the regeneration of neurons exposed to the differential conditioned media (Figure 7), this may be explained by the very small magnitude of increased NGF expression ( $\approx 1 \text{ ng mL}^{-1}$ ) resulting from an individual's sAD-MSC exposed to GO substrate (see Figure S4, Supporting Information). Concentration differences in GDNF secretion were even less prominent ( $< 0.5 \text{ ng mL}^{-1}$ ). By contrast, functional differences in PC12 cell-line neurite sprouting have previously been observed to require exogenous NGF doses greater than  $66 \text{ ng mL}^{-1}$ .<sup>[40]</sup> We undertook an indirect conditioned media model to eliminate the preferential regeneration of DRG observed on graphene materials;<sup>[41]</sup> however, it fails to replicate the complex *in vivo* milieu which demands cross-talk of cells and the regenerating neuron to fulfill dynamic trophic secretion;<sup>[42]</sup> therefore the true effect may be masked.

Severe PNIs comprise harsh environments that trigger cell detachment from conduit surfaces which was modeled by exposing sAD-MSCs on GO substrates to PBS (Figure 8).<sup>[43]</sup> Following 30 min-exposure, sAD-MSC on GO substrates had increased cell numbers and metabolic activity compared to glass. GO substrates confer resistance to detachment for cells under other destructive environmental cues such as shear force, indicating it is a desirable substrate for stress conditions where anoikis occurs.<sup>[44]</sup> Our transcriptome data demonstrates upregulated ECM-related genes that may explain improved viability, including collagen, which plays a crucial role in MSC adhesion

and survival under H<sub>2</sub>O<sub>2</sub> stress.<sup>[45,46]</sup> Enhancing sAD-MSC survival in severe PNI conditions may provide a significant therapeutic advantage that merits future *in vivo* experiments.

The stable properties of GO substrates coupled with their influence on sAD-MSC to increase neurotrophin secretion and resistance to cell death under stressful conditions indicate that they are a promising intervention to augment cell therapy in severe PNI.

## Supporting Information

Supporting Information is available from the Wiley Online Library or from the author.

## Acknowledgements

S.H.L and A.V. acknowledge funding support from the Engineering and Physical Science Research Council (EPSRC) Grant No. EP/L01548X/1 and the Graphene NOWNANO Centre for Doctoral Training. A.F. and A.J.R. were supported by the Hargreaves and Ball Trust, the Academy of Medical Sciences (AMS-SGCL7), and by Seed Corn funding from the Rosetrees Trust and the Stonegate Trust (M746). The authors thank Acorda Therapeutics for kindly supplying them with the recombinant GGF-2 used in this study. The authors also thank Rachel Scholey, Leo Zeef, and Andy Hayes of the Bioinformatics and Genomic Technologies Core Facilities at The University of Manchester for providing support with regard to RNA-seq. The authors would also like to acknowledge the assistance given by IT Services and the use of the Computational Shared Facility at The University of Manchester.

## Conflict of Interest

The authors declare no conflict of interest.

## Data Availability Statement

The data that support the findings of this study are openly available in ArrayExpress at <https://www.ebi.ac.uk/arrayexpress/>, reference number E-MTAB-10078.

## Keywords

adipose stem cells, graphene oxide, nerve regeneration, peripheral nerve injuries, Schwann cells

Received: September 10, 2020

Revised: February 4, 2021

Published online: March 4, 2021

- [1] K. R. Jessen, R. Mirsky, *Front. Cell. Neurosci.* **2019**, *13*, 33.
- [2] A. Niapour, F. Karamali, K. Karbalaie, A. Kiani, M. Mardani, M. H. Nasr-Esfahani, H. Baharvand, *Biotechnol. Lett.* **2010**, *32*, 781.
- [3] A. Musiał-Wysocka, M. Kot, M. Majka, *Cell Transplant.* **2019**, *28*, 801.
- [4] R. Dai, Z. Wang, R. Samanipour, K. I. Koo, K. Kim, *Stem Cells Int.* **2016**, *2016*, 6737345.
- [5] K. Tomita, T. Madura, Y. Sakai, K. Yano, G. Terenghi, K. Hosokawa, *Neuroscience* **2013**, *236*, 55.

- [6] R. Piovesana, A. Faroni, V. Magnaghi, A. J. Reid, A. M. Tata, *Cell Death Discovery* **2019**, *5*, 92.
- [7] K. Tomita, T. Madura, C. Mantovani, G. Terenghi, *J. Neurosci. Res.* **2012**, *90*, 1392.
- [8] A. Faroni, R. J. P. Smith, L. Lu, A. J. Reid, *Eur. J. Neurosci.* **2016**, *43*, 417.
- [9] P. Erba, C. Mantovani, D. F. Kalbermatten, G. Pierer, G. Terenghi, P. J. Kingham, *J. Plast. Reconstr. Aesthetic Surg.* **2010**, *63*, e811.
- [10] M. J. Dalby, N. Gadegaard, R. Tare, A. Andar, M. O. Riehle, P. Herzyk, C. D. W. Wilkinson, R. O. C. Oreffo, *Nat. Mater.* **2007**, *6*, 997.
- [11] A. Dolatshahi-Pirouz, T. Jensen, D. C. Kraft, M. Foss, P. Kingshott, J. L. Hansen, A. N. Larsen, J. Chevallier, F. Besenbacher, *ACS Nano* **2010**, *4*, 2874.
- [12] S. R. Shin, Y.-C. Li, H. L. Jang, P. Khoshakhlagh, M. Akbari, A. Nasajpour, Y. S. Zhang, A. Tamayol, A. Khademhosseini, *Adv. Drug Delivery Rev.* **2016**, *105*, 255.
- [13] J. Wang, W. Zheng, L. Chen, T. Zhu, W. Shen, C. Fan, H. Wang, X. Mo, *ACS Biomater. Sci. Eng.* **2019**, *5*, 2444.
- [14] W. C. Lee, C. H. Y. X. Lim, H. Shi, L. A. L. Tang, Y. Wang, C. T. Lim, K. P. Loh, *ACS Nano* **2011**, *5*, 7334.
- [15] S. D. Newby, T. Masi, C. D. Griffin, W. J. King, A. Chipman, S. Stephenson, D. E. Anderson, A. S. Biris, S. E. Bourdo, M. Dhar, *Int. J. Nanomed.* **2020**, *15*, 2501.
- [16] A. F. Verre, A. Faroni, M. Iliut, C. Silva, C. Muryn, A. J. Reid, A. Vijayaraghavan, *Interface Focus* **2018**, *8*, 20180002.
- [17] J. K. Wychowaniec, M. Iliut, M. Zhou, J. Moffat, M. A. Elsayy, W. A. Pinheiro, J. A. Hoyland, A. F. Miller, A. Vijayaraghavan, A. Saiani, *Biomacromolecules* **2018**, *19*, 2731.
- [18] I. Horcas, R. Fernández, J. M. Gómez-Rodríguez, J. Colchero, J. Gómez-Herrero, A. M. Baro, *Rev. Sci. Instrum.* **2007**, *78*, 013705.
- [19] A. Kovtun, D. Jones, S. Dell'Elce, E. Treossi, A. Liscio, V. Palermo, *Carbon* **2019**, *143*, 268.
- [20] M. Dominici, K. L. Blanc, I. Mueller, I. Slaper-Cortenbach, F. Marini, D. S. Krause, R. J. Deans, A. Keating, D. J. Prockop, E. M. Horwitz, *Cytotherapy* **2006**, *8*, 315.
- [21] FastQC: A Quality Control Tool for High Throughput Sequence Data, <http://www.bioinformatics.babraham.ac.uk/projects/fastqc/> (accessed: October 2019).
- [22] A. M. Bolger, M. Lohse, B. Usadel, *Bioinformatics* **2014**, *30*, 2114.
- [23] A. Dobin, C. A. Davis, F. Schlesinger, J. Drenkow, C. Zaleski, S. Jha, P. Batut, M. Chaisson, T. R. Gingeras, *Bioinformatics* **2013**, *29*, 15.
- [24] M. I. Love, W. Huber, S. Anders, *Genome Biol.* **2014**, *15*, 550.
- [25] A. C. de Luca, A. Faroni, A. J. Reid, *J. Visualized Exp.* **2015**, *96*, e52543.
- [26] K. Ganesan, S. Ghosh, N. G. Krishna, S. Ilango, M. Kamruddin, A. K. Tyagi, *Phys. Chem. Chem. Phys.* **2016**, *18*, 22160.
- [27] E.-S. Kang, I. Song, D.-S. Kim, U. Lee, J.-K. Kim, H. Son, J. Min, T.-H. Kim, *Colloids Surf., B* **2018**, *169*, 20.
- [28] J. Kim, H. D. Kim, J. Park, E. Lee, E. Kim, S. S. Lee, J.-K. Yang, Y.-S. Lee, N. S. Hwang, *Biomater. Res.* **2018**, *22*, 1.
- [29] X. Shi, H. Chang, S. Chen, C. Lai, A. Khademhosseini, H. Wu, *Adv. Funct. Mater.* **2012**, *22*, 751.
- [30] J. M. Gimble, B. A. Bunnell, T. Frazier, B. Rowan, F. Shah, C. Thomas-Porch, X. Wu, *Organogenesis* **2013**, *9*, 3.
- [31] W. M. Harris, P. Zhang, M. Plastini, T. Ortiz, N. Kappy, J. Benites, E. Alexeev, S. Chang, R. Brockunier, J. P. Carpenter, S. A. Brown, *Cytotherapy* **2017**, *19*, 211.
- [32] M. Tang, J. Li, L. He, R. Guo, X. Yan, D. Li, Y. Zhang, M. Liao, B. Shao, Y. Hu, Y. Liu, Q. Tang, L. Xia, X. Guo, R. Chai, *Colloids Surf., B* **2019**, *182*, 110324.
- [33] S. Gao, Y. Zheng, Q. Cai, X. Wu, W. Yao, J. Wang, *Arch. Med. Sci.* **2015**, *11*, 886.
- [34] H. Orbay, C. J. Little, L. Lankford, C. A. Olson, D. E. Sahar, *Ann. Plast. Surg.* **2015**, *74*, 584.
- [35] A. E. Mortimer, A. Faroni, M. A. Kilic, A. J. Reid, *Stem Cells Int.* **2017**, *2017*, 1479137.
- [36] J. E. Tomlinson, E. Žygelytė, J. K. Grenier, M. G. Edwards, J. Cheetham, *J. Neuroinflammation* **2018**, *15*, 185.
- [37] S. R. Das, M. Uz, S. Ding, M. T. Lentner, J. A. Hondred, A. A. Cargill, D. S. Sakaguchi, S. Mallapragada, J. C. Claussen, *Adv. Healthcare Mater.* **2017**, *6*, 1601087.
- [38] D. Mahay, G. Terenghi, S. G. Shawcross, *Exp. Cell Res.* **2008**, *314*, 2692.
- [39] X. Fang, L. Djouhri, S. McMullan, C. Berry, S. G. Waxman, K. Okuse, S. N. Lawson, *J. Neurosci.* **2006**, *22*, 7425.
- [40] X. Cao, M. Shoichet, *Neuroscience* **2001**, *103*, 831.
- [41] D. Convertino, S. Luin, L. Marchetti, C. Coletti, *Front. Neurosci.* **2018**, *12*, 1.
- [42] K.-H. Tse, L. N. Novikov, M. Wiberg, P. J. Kingham, *Exp. Cell Res.* **2015**, *331*, 142.
- [43] P. G. di Summa, D. F. Kalbermatten, W. Raffoul, G. Terenghi, P. J. Kingham, *Tissue Eng., Part A* **2013**, *19*, 368.
- [44] J. Vlček, L. Lapčík, M. Havrdová, K. Poláková, B. Lapčíková, T. Opletal, J. P. Froning, M. Otyepka, *Nanoscale* **2019**, *11*, 3222.
- [45] C. Somaiah, A. Kumar, D. Mawrie, A. Sharma, S. D. Patil, J. Bhattacharyya, R. Swaminathan, B. G. Jaganathan, *PLoS One* **2015**, *10*, e0145068.
- [46] J. Park, B. Kim, J. Han, J. Oh, S. Park, S. Ryu, S. Jung, J.-Y. Shin, B. S. Lee, B. H. Hong, D. Choi, B.-S. Kim, *ACS Nano* **2015**, *9*, 4987.